Probabilistic Analysis and Design of Circular Tunnels against Face Stability

Guilhem Mollon, Dias Daniel, Abdul-Hamid Soubra

Probabilistic Analysis and Design of Circular Tunnels against Face Stability

Guilhem Mollon[1]; Daniel Dias[2]; and Abdul-Hamid Soubra, M.ASCE[3]

Abstract: This paper presents a reliability-based approach for the three-dimensional analysis and design of the face stability of a shallow circular tunnel driven by a pressurized shield. Both the collapse and the blow-out failure modes of the ultimate limit state are studied. The deterministic models are based on the upper-bound method of the limit analysis theory. The collapse failure mode was found to give the most critical deterministic results against face stability and was adopted for the probabilistic analysis and design. The random variables used are the soil shear strength parameters. The Hasofer-Lind reliability index and the failure probability were determined. A sensitivity analysis was also performed. It was shown that (1) the assumption of negative correlation between the soil shear strength parameters gives a greater reliability of the tunnel face stability with respect to the one of uncorrelated variables; (2) FORM approximation gives accurate results of the failure probability; and (3) the failure probability is much more influenced by the coefficient of variation of the angle of internal friction than that of the cohesion. Finally, a reliability-based design is performed to determine the required tunnel pressure for a target collapse failure probability.

DOI: 10.1061/(ASCE)1532-3641(2009)9:6(237)

CE Database subject headings: Tunnels; Pressure; Passive pressure; Limit analysis; Probability; Design.

Introduction

Over the past 30 years, tunneling in a frictional and/or cohesive soil has been possible due to recent technological advances including the pressurized shield. Face stability analysis of shallow circular tunnels driven by the pressurized shield is of major importance. The tunnel face pressure must avoid both the collapse (active failure) and the blow-out (passive failure) of the soil mass nearby the tunnel face. Active failure of the tunnel is triggered by application of surcharge and self-weight, with the tunnel face pressure providing resistance against collapse. Under passive conditions, these roles are reversed and the face pressure causes blow-out with resistance being provided by the surcharge and self-weight.

In this paper, the face stability analysis is conducted based on a probabilistic approach. The reliability-based analysis is more rational than the deterministic one since it takes into account the inherent uncertainty of the input variables. Nowadays, this is possible because of the improvement of our knowledge on the statistical properties of the soil (Phoon and Kulhawy 1999; Baecher and Christian 2003). Two performance functions may characterize the tunnel behavior: the serviceability limit state and the ultimate limit state (ULS). Only the collapse and the blow-out failure modes of the ULS are analyzed herein. Two new rigorous deterministic limit analysis models are used. The soil shear strength parameters are modeled as random variables. The main reliability concepts are described next, followed by the two deterministic models and discussions of the deterministic and probabilistic numerical results based on these models.

[1]Ph.D. Student, INSA Lyon, LGCIE Site Coulomb 3, Géotechnique, Bât. J.C.A. Coulomb, Domaine scientifique de la Doua, 69621 Villeurbanne cedex, France. E-mail: Guilhem.Mollon@insa-lyon.fr

[2]Associate Professor, INSA Lyon, LGCIE Site Coulomb 3, Géotechnique, Bât. J.C.A. Coulomb, Domaine scientifique de la Doua, 69621 Villeurbanne cedex, France. Email: Daniel.Dias@insa-lyon.fr

[3]Professor, Dept. of Civil Engineering, Univ. of Nantes, Bd. de l'université, BP 152, 44603 Saint-Nazaire, France (corresponding author). E-mail: Abed.Soubra@univ-nantes.fr

Note. This manuscript was submitted on April 25, 2008; approved on July 1, 2009; published online on November 13, 2009. Discussion period open until May 1, 2010; separate discussions must be submitted for individual papers. This paper is part of the ***International Journal of Geomechanics***, Vol. 9, No. 6, December 1, 2009. ©ASCE, ISSN 1532-3641/2009/6-237–249/$25.00.

Overview of Reliability Concepts

The reliability index is a measure of the safety that takes into account the inherent uncertainties of the input variables. A widely used reliability index is the Hasofer and Lind (1974) index. Its matrix formulation is (Ditlevsen 1981)

$$\beta_{HL} = \min_{x \in F} \sqrt{(x-\mu)^T C^{-1} (x-\mu)} \quad (1)$$

in which x=vector representing the n random variables; μ =vector of their mean values; C=covariance matrix; and F =failure region. The minimization of Eq. (1) is performed subject to the constraint $G(x) \leqslant 0$ where the limit state surface $G(x)=0$, separates the n dimensional domain of random variables into two regions: a failure region F represented by $G(x) \leqslant 0$ and a safe region given by $G(x) > 0$.

The classical approach for computing β_{HL} by Eq. (1) is based on the transformation of the limit state surface into the rotated space of standard normal uncorrelated variates. The shortest distance from the transformed failure surface to the origin of the reduced variates is the reliability index β_{HL}.

An intuitive interpretation of the reliability index was suggested in Low and Tang (1997a, 2004) where the concept of an expanding ellipsoid [or an ellipse in two-dimensions (2D) as shown in Fig. 1] led to a simple method of computing the Hasofer-Lind reliability index in the original space of the random

Int. J. Geomech. 2009.9:237-249.

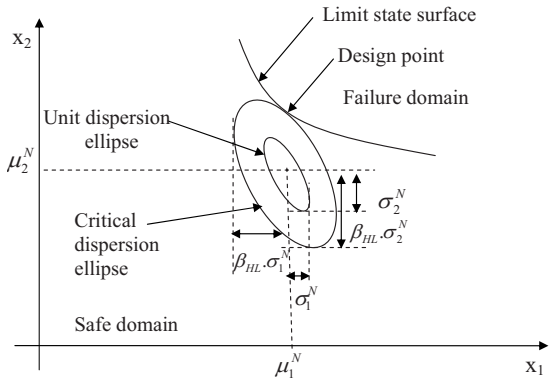

Fig. 1. Design point and equivalent normal dispersion ellipses in the space of two random variables

variables using an optimization tool available in most software packages. Low and Tang (1997a,2004) reported that the Hasofer-Lind reliability index β_{HL} may be regarded as the codirectional axis ratio of the smallest ellipsoid that just touches the limit state surface to the unit dispersion ellipsoid [i.e., corresponding to $\beta_{HL}=1$ in Eq. (1) without the minimum]. They also stated that finding the smallest ellipsoid (called hereafter critical ellipsoid) that is tangent to the limit state surface is equivalent to finding the most probable failure point. When the random variables are non-normal, the Rackwitz-Fiessler equivalent normal transformation was used to compute the equivalent normal mean μ^N and the equivalent normal standard deviation σ^N. The iterative computations of μ^N and σ^N for each trial design point are automatic during the constrained optimization search.

From the first-order reliability method FORM and the Hasofer-Lind reliability index β_{HL}, one can approximate the failure probability as follows:

$$P_f \approx \Phi(-\beta_{HL}) \tag{2}$$

where $\Phi(\cdot)$=cumulative distribution function of a standard normal variable. In this method, the limit state function is approximated by a hyperplane tangent to the limit state surface at the design point.

Monte Carlo (MC) is another method of computing the failure probability. It is the most robust simulation method in which samples are generated with respect to the probability density of each variable. For each sample, the response of the system is calculated. An unbiased estimator of the failure probability is given by

$$\tilde{P}_f = \frac{1}{N}\sum_{i=1}^{N} I(x_i) \tag{3}$$

where N=number of samples and $I(x)=1$ if $G(x)\leq 0$ and 0 elsewhere. The coefficient of variation of the estimator is given by

$$\mathrm{COV}(\tilde{P}_f) = \sqrt{\frac{(1-P_f)}{P_f N}} \tag{4}$$

Generally, for a given target of the coefficient of variation, the crude MC simulation requires a large number of samples, i.e., a large computation time. This is especially the case for small values of the failure probability. The importance sampling (IS) simulation method is a more efficient approach; it requires fewer sample points than the MC method. In this approach, the initial sampling density $f(\cdot)$ is shifted to the design point in order to concentrate the samples in the region of greatest probability density within the zone defined by $G(x)\leq 0$. The design point may be determined by using any of the classical methods such as Rackwitz-Fiessler algorithm (Rackwitz and Fiessler 1978), Low and Tang's ellipsoid approach (Low and Tang 1997a, 2004), etc. An estimator of the failure probability P_f is obtained as follows (Melchers 1999):

$$\tilde{P}_f = \frac{1}{N}\sum_{i=1}^{N} I(v_i)\frac{f(v_i)}{h(v_i)} \tag{5}$$

where $h(\cdot)$=new sampling density centered at the design point and v=vector of sample values generated with the new probability density function (PDF), i.e., $h(\cdot)$. The coefficient of variation of the estimator is given by (Melchers 1999)

$$\mathrm{COV}(\tilde{P}_f) = \frac{1}{P_f}\sqrt{\frac{1}{N}\left(\frac{1}{N}\sum_{i=1}^{N}\left(I(v_i)\frac{f(v_i)}{h(v_i)}\right)^2 - (P_f)^2\right)} \tag{6}$$

Reliability Analysis of a Circular Tunnel Face

The aim of this paper is to perform a reliability analysis of the face stability of a shallow circular tunnel driven by a pressurized shield in a c-φ soil. The problem can be idealized as shown in Figs. 2(a and b) by considering a circular rigid tunnel of diameter D driven under a depth of cover C. A surcharge σ_s is applied at the ground surface and a uniform retaining pressure σ_t is applied to the tunnel face to simulate tunneling under compressed air. The deterministic models are based on the upper-bound method of the limit analysis theory. They are presented in the next section. Due to uncertainties in soil shear strength parameters, the cohesion c, and the angle of internal friction φ are considered as random. They are modeled in the present analysis as random variables. This means that the soil parameters are considered as homogeneous in the whole soil mass. The randomness of the soil is taken into account from one simulation to another. The performance functions G_1 and G_2 used in the reliability analysis for both the collapse and the blow-out cases are respectively defined as follows:

$$G_1 = \sigma_t - \sigma_c \tag{7}$$

$$G_2 = \sigma_b - \sigma_t \tag{8}$$

where σ_t=applied pressure on the tunnel face, and σ_c and σ_b=collapse and blow-out pressures, respectively.

Limit Analysis Models

Several theoretical models have been presented in literature for the computation of the collapse and blow-out tunnel pressures corresponding respectively to the active and passive modes of failure. The most recent and significant approach is the one presented by Leca and Dormieux (1990) who considered three-dimensional (3D) failure mechanisms in the framework of the upper-bound method in limit analysis. In this paper, two new deterministic models (3D multiblock failure mechanisms) based on the upper-bound approach of limit analysis are proposed for the probabilistic analysis. These mechanisms constitute an improvement of the failure mechanisms by Leca and Dormieux (1990) since they allow the 3D slip surface to develop more freely in comparison with the available one- and two-block mechanisms

Int. J. Geomech. 2009.9:237-249.

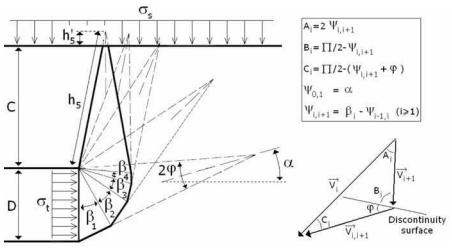

a. M1 mechanism (collapse case) in the (y, z) plane

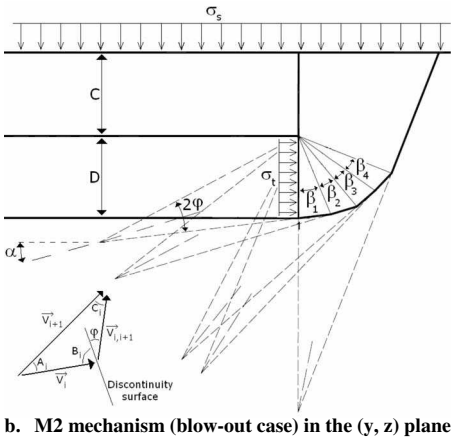

b. M2 mechanism (blow-out case) in the (y, z) plane

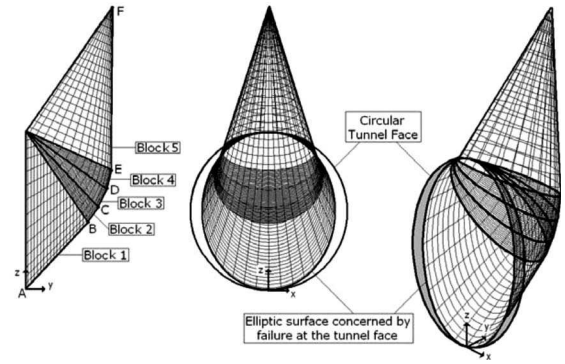

c. Three-dimensional views of the M1 mechanism in the (x, y, z) space

Fig. 2. Failure mechanisms M1 and M2 for the face stability

given by Leca and Dormieux (1990). Notice that the use of a lower-bound approach in limit analysis (using for instance finite elements and linear programming) is another alternative approach. It has the advantage of providing conservative solutions. However, this method leads, when dealing with the probabilistic analysis, to complex and very expensive numerical computations with a high computation time since the probabilistic analysis requires a significant number of calls of the deterministic model for a given soil variability. Thus, in order to optimize the computation time and to get sufficiently accurate results, efforts were concentrated in the present paper on the improvement of the best available upper-bound solutions (i.e., those by Leca and Dormieux 1990) by using multiblock failure mechanisms. Notice that a multiblock failure mechanism was also used by Soubra (1999) when dealing with the 2D analysis of the bearing capacity of strip foundations. It was shown by Soubra (1999) that the multiblock mechanism significantly improves the solutions of the bearing capacity as given by the available mechanisms (two-block and log-sandwich mechanisms) and obtains smaller (i.e., better) upper bounds. This is due to the great freedom offered by this mechanism to move more freely with respect to traditional mechanisms.

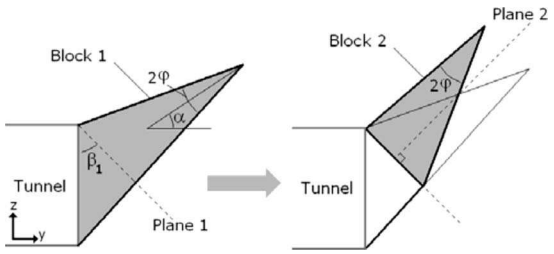

Fig. 3. Detail of the construction of the M1 mechanism in the (y,z) plane

The optimal radial shear zone found in the case of a ponderable soil was not bounded by a log spiral as is the case of the traditional Prandtl (i.e., log sandwich) mechanism but by a more critical surface found by numerical optimization. Furthermore, the multiblock mechanism by Soubra (1999) led in some cases (for N_q and N_c) to the exact solutions given by the log-sandwich failure mechanism since both upper and lower bound solutions were identical in these cases. Notice finally that the two 3D multiblock failure mechanisms presented in this paper for the stability analysis of circular tunnels make use of the idea of multiblock mechanisms suggested by Soubra (1999) in the 2D analysis of strip footings in order to obtain better upper-bound solutions. A detailed description of these mechanisms is given in the following sections.

Collapse Mechanism M1 (Active Case)

M1 is an improvement of the two-block collapse mechanism presented by Leca and Dormieux (1990). This mechanism is a multiblock. It is composed of n truncated rigid cones with circular cross sections and with opening angles equal to 2φ. Fig. 2(c) depicts three different 3D views of a five-block mechanism (i.e., $n=5$). The geometrical construction of this mechanism is similar to that of Leca and Dormieux (1990), i.e., each cone is the mirror image of the adjacent cone with respect to the plane that is normal to the contact surface separating these cones (cf. Leca and Dormieux 1990). This is a necessary condition to assure the same elliptical contact area between adjacent cones. In order to make clearer the geometrical construction of the 3D failure mechanism, Fig. 3 shows how the first two truncated conical blocks adjacent to the tunnel face are constructed. The geometrical construction of the remaining truncated conical blocks is straightforward. In Fig. 3, Block 1 is a truncated circular cone adjacent to the tunnel face. It has an opening angle equal to 2φ (in order to respect the normality condition in limit analysis) and an axis inclined at α with the horizontal direction. Thus, the intersection of this truncated cone with the tunnel face is an elliptical surface that does not cover the entire circular face of the tunnel [cf. Fig. 2(c)] This is a shortcoming not only of the present failure mechanism but also of the one- and two-block mechanisms by Leca and Dormieux (1990). On the other hand, Block 1 is truncated with Plane 1, which is inclined at an angle β_1 with the vertical direction (cf. Fig. 3). In order to obtain the same contact area with the adjacent truncated conical block, Block 2 is constructed in such a manner to be the mirror image of Block 1 with respect to the plane that is normal to the surface separating the two blocks (i.e., Plane 2 as shown in Fig. 3). The upper rigid cone will or will not intersect the ground surface depending on the φ and C/D values. At first glance, the fact that the failure mechanism does not intersect the ground surface for some values of φ and C/D is striking. However, the same phenomenon was also observed

Int. J. Geomech. 2009.9:237-249.

when performing 3D numerical simulations using FLAC^{3D} software (Mollon et al. 2009). Notice that while using numerical simulations, no assumptions were made on the shape of the failure mechanism and the optimal failure mechanism was explored. Thus, one may confirm that the present failure mechanism based on limit analysis is acceptable even if the critical failure surface does not outcrop.

M1 is a translational kinematically admissible failure mechanism. The different truncated conical blocks of this mechanism move as rigid bodies. These truncated rigid cones translate with velocities of different directions, which are collinear with the cones axes and make an angle φ with the conical discontinuity surface in order to respect the normality condition required by the limit analysis theory. The velocity of each cone is determined by the condition that the relative velocity between the cones in contact has the direction that makes an angle φ with the contact surface. The velocity hodograph is presented in Fig. 2(a). The present mechanism is completely defined by n angular parameters α and β_i $(i=1,\ldots,n-1)$ where n is the number of the truncated conical blocks.

Blow-Out Mechanism M2 (Passive Case)

Even though safety against collapse is a major concern during tunneling, the blow-out mechanism may be of interest for very shallow tunnels bored in weak soils, when the pressure σ_t can become so great that soil is heaved in front of the shield. M2 [Fig. 2(b)] is a blow-out mechanism. It represents the passive case of the former mechanism. With reference to M1, the M2 mechanism presents an upward movement of the soil mass. Thus, the cones with an opening angle 2φ are reversed. Contrary to M1, the present mechanism always outcrops.

Ellipsoid Approach via Spreadsheet

In the present paper, by the Low and Tang (1997a, 2004) method, one literally sets up a tilted ellipsoid in the Excel spreadsheet and minimizes the dispersion ellipsoid subject to the constraint that it be tangent to the limit state surface using the Excel Solver with the automatic scaling option. Eq. (1) may be rewritten as (Low and Tang 1997b, 2004; Youssef Abdel Massih and Soubra 2008; Youssef Abdel Massih et al. 2008)

$$\beta_{HL} = \min_{x \in F} \sqrt{\left[\frac{x-\mu^N}{\sigma^N}\right]^T [R]^{-1} \left[\frac{x-\mu^N}{\sigma^N}\right]} \tag{9}$$

in which $[R]^{-1}$=inverse of the correlation matrix. This equation will be used [instead of Eq. (1)] since the correlation matrix $[R]$ displays the correlation structure more explicitly than the covariance matrix $[C]$.

Deterministic Numerical Results

For both M1 and M2 mechanisms, when the total rate of energy dissipation and the total rate of external work are equated, the ultimate tunnel pressure σ_u for the collapse and the blow-out modes of failure can be expressed as follows:

$$\sigma_u = \gamma D N_\gamma + c N_c + \sigma_s N_s \tag{10}$$

where N_γ, N_c, and N_s=nondimensional coefficients. They represent, respectively, the effect of soil weight, cohesion, and surcharge loading. The expressions of the different coefficients N_γ, N_c, and N_s are given in the Appendix. Notice that the external forces involved in the present mechanisms are the weights of the different truncated rigid cones, the surcharge loading acting on the ground surface, and the pressure applied on the tunnel face. For the collapse mechanism, the rate of external work of the surcharge loading should be calculated only in case of outcrop of the mechanism on the ground surface. The computation of the rate of external work of the different external forces is straightforward. The details are given in Oberlé (1996). The rate of internal energy dissipation takes place along the different velocity discontinuity surfaces. These are (1) the radial elliptical surfaces which are the contact areas between adjacent truncated cones and (2) the lateral surfaces of the different truncated cones. Notice that the rate of internal energy dissipation along a unit velocity discontinuity surface is equal to $c \cdot \delta u$ (Chen 2008) where c is the soil cohesion and δu is the tangential component of the velocity along the velocity discontinuity surface. Calculations of the rate of internal energy dissipation along the different velocity discontinuity surfaces are straightforward. The details are given in Oberlé (1996).

In Eq. (10), σ_u, N_γ, N_c, and N_s depend not only on the mechanical and geometrical characteristics c, φ, and C/D, but also on the angular parameters of the failure mechanism α and β_i $(i=1,\ldots,n-1)$. In the following sections, the ultimate tunnel pressure of the collapse mode will be denoted σ_c, and that of blow-out will be refereed to as σ_b. They were obtained respectively by maximization and minimization of σ_u in Eq. (10) with respect to the α and β_i angles. As for the ultimate tunnel pressures, the critical coefficients N_γ^b, N_c^b, and N_s^b (respectively N_γ^c, N_c^c, and N_s^c) corresponding to the blow-out (respectively collapse) case, were obtained by minimization (respectively maximization) of these coefficients with respect to the α and β_i angles. A computer program has been written in Microsoft Excel Visual Basic to define the different coefficients N_γ, N_c, and N_s and the tunnel pressure σ_u for the collapse and the blow-out modes of failure. The optimization was performed using the optimization tool "Solver" implemented in Microsoft Excel. It was shown that the increase in the number of cones improves the solutions (i.e., increases the active coefficients, and reduces the passive ones). The numerical results have shown that this improvement becomes insignificant (smaller than 1%) for a number of blocks greater than five. Therefore, only five blocks were used in this paper for the collapse and the blow-out mechanisms.

Notice that in both the collapse and the blow-out cases, the numerical results have shown that N_c and N_s are related by the following classical formula:

$$N_c \tan\varphi + 1 - N_s = 0 \tag{11}$$

This can be explained by the theorem of corresponding states (Soubra 1999). Hence, in the following, only the N_γ and N_s coefficients will be presented; the N_c coefficient can be obtained using Eq. (11).

Comparison with Available Upper-Bound Solutions

Leca and Dormieux (1990) have considered a collapse failure mechanism composed of two rigid cones. Fig. 4 presents the N_γ^c and N_s^c values given by the present analysis (M1 mechanism) and the ones given by Leca and Dormieux (1990). The N_γ^c coefficient increases with C/D; then, it becomes constant for large values of C/D corresponding to the condition of no outcrop of the upper block. However, coefficient N_s^c decreases with the C/D increase and vanishes beyond a certain value of C/D corresponding to the no-outcrop condition. In this case, the surcharge loading has no

Int. J. Geomech. 2009.9:237-249.

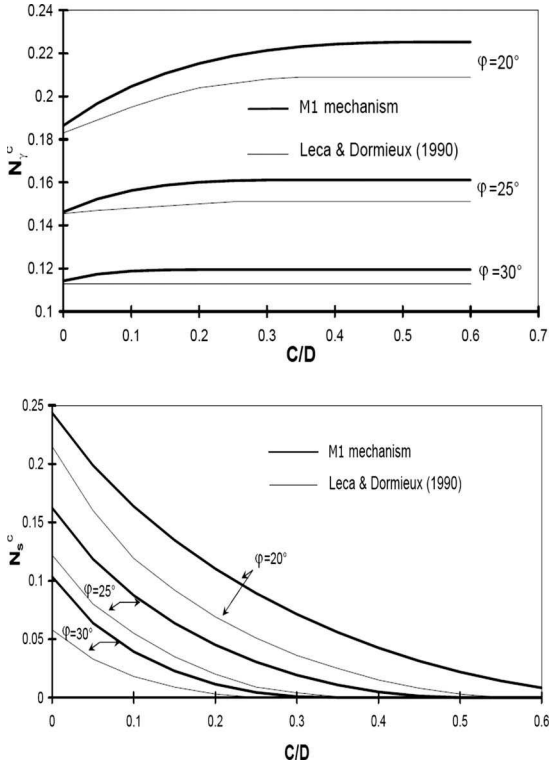

Fig. 4. N_γ^c and N_s^c versus C/D as given by Leca and Dormieux and M1 mechanism

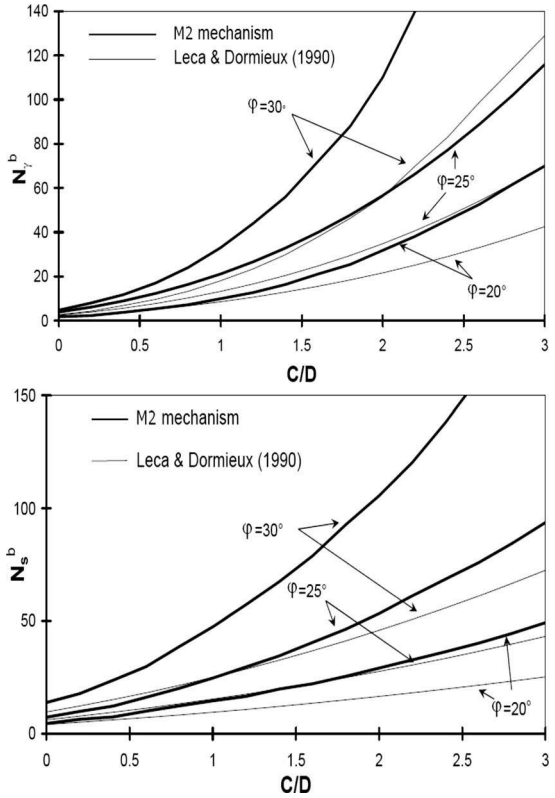

Fig. 5. N_γ^b and N_s^b versus C/D as given by Leca and Dormieux and M2 mechanism

influence on the critical N_s^c value. These conclusions conform to those of Leca and Dormieux (1990). It should be mentioned that in the case of collapse, the present failure mechanism gives greater upper-bound solutions than the available upper-bound solutions proposed by Leca and Dormieux (1990). The improvement of the solution is about 8% for the N_γ^c coefficient when $\varphi=20°$ and $C/D>0.55$. For N_s^c, the improvement is equal to 37.5% when $\varphi=20°$ and $C/D=0.1$.

For the blow-out case, Leca and Dormieux (1990) have considered a mechanism composed of a single rigid cone moving upward. The upper-bound solutions given by these writers are compared with the ones corresponding to the present M2 mechanism in Fig. 5. The M2 mechanism is better than the one presented by Leca and Dormieux (1990) since the present upper-bound solutions are smaller. For the N_γ^b coefficient, the reduction is very significant and it is of 41% when $\varphi=30°$ and $C/D=1.4$. For the N_s^b coefficient, significant reductions are also obtained with respect to the results presented by Leca and Dormieux. For example, when $\varphi=30°$ and $C/D=1.4$, the reduction attains 51%.

As a conclusion, the four design charts presented before (i.e., Figs. 4 and 5) give the values of the coefficients N_γ and N_s of the proposed mechanisms for both the collapse and blow-out cases for different values of the governing parameters φ and C/D. The existing values by Leca-Dormieux are also given in these charts, allowing one to appreciate the improvement with respect to prior solutions. The determination of the critical collapse or blow-out pressure to be used in practice can then be made by using Eq. (10) where N_c in this equation is given by Eq. (11) and N_γ and N_s are given in the design charts of Figs. 4 and 5.

It should be mentioned here that Fig. 2(c) presented earlier is a 3D representation of the critical collapse mechanism obtained after optimization of the tunnel pressure with respect to the geometrical parameters of the failure mechanism for a friction angle equal to 17° and a cohesion equal to 7 kPa when $C/D=2$. It can be seen that the 3D critical failure mechanism M1 involves a radial shear zone (composed of three small truncated rigid cones, i.e., Blocks 2–4) sandwiched between two greater rigid cones (i.e., Blocks 1 and 5). Line BCDE as obtained by numerical optimization is not a log spiral and this constitutes the major interest of the present multiblock mechanism with respect to the similar in shape mechanism (i.e., log sandwich) where line BCDE is replaced by a log spiral.

For the currently encountered cases (i.e., $1\leqslant C/D\leqslant 3$; $10°\leqslant\varphi\leqslant 30°$; $0\leqslant c\leqslant 20$ kPa), Table 1 presents the results of the tunnel ultimate pressures σ_c and σ_b corresponding respectively to the collapse and the blow-out modes of failure as given by the present failure mechanisms. The applied tunnel pressure σ_t should be greater than the collapse pressure σ_c to avoid the active failure. If one adopts a safety factor against collapse ($F_s=\sigma_t/\sigma_c$) equal to 2, the required applied pressure σ_t should be equal to twice the value of the collapse pressure as given in the fifth column of Table 1. The comparison of these pressures with those of the blow-out case (i.e., σ_b) shows that the blow-out pressures are much higher than the practical applied tunnel pressures σ_t for all the values of the governing parameters considered in this paper. Hence, the blow-out mode of failure does not occur for the cases currently encountered in practice. In the following sections, only the collapse failure mode is considered in the probabilistic analysis and design of circular tunnels against face stability.

Comparison with Three-Dimensional Numerical Simulations

In order to assess the accuracy of the limit analysis collapse model, complex 3D numerical simulations were performed using

Int. J. Geomech. 2009.9:237-249.

Table 1. Values of the Collapse and Blow-Out Pressures σ_c and σ_b and the Required Face Pressure σ_t for a Safety Factor $F_s=2$ for the Common Values of C/D, φ, and c

C/D	φ (°)	c (kPa)	σ_c (kPa)	σ_t (kPa) for $F_s=2$	σ_b (kPa)
1	10	0	100	200	660
1	10	20	<0 (i.e., stable)	<0 (i.e., stable)	94
1	30	0	22	44	3,800
1	30	20	<0 (i.e., stable)	<0 (i.e., stable)	4,700
3	10	0	106	212	2,570
3	10	20	<0 (i.e., stable)	<0 (i.e., stable)	3,290
3	30	0	22	44	20,900
3	30	20	<0 (i.e., stable)	<0 (i.e., stable)	23,400

the finite difference commercial software FLAC^{3D}. They allow one to determine the values of the critical collapse pressure σ_c. For a detailed description of these simulations, the reader may refer to Mollon et al. (2009) . Fig. 6(a) shows a comparison between the collapse pressures as given by the FLAC^{3D} model and by the M1 mechanism. Three cases of (c,φ) are considered to show the effect of both c and φ on the comparison between the limit analysis and the numerical simulations. It appears that the limit analysis results are not far from the ones obtained by FLAC^{3D}. Even if they are upper-bounds (i.e., nonconservative) to the exact collapse pressures, the present collapse pressures given by limit analysis can be considered as sufficiently accurate for practical use. Notice also that the very short calculation time required by the limit analysis model (smaller than 1 s) compared to that required by the numerical simulations (90 min) is appealing for the probabilistic analysis, which requires a significant number of calls of the deterministic model for a given soil variability. Finally, Fig. 6(b) shows that the shape of the critical M1 collapse mechanism is very close to the one obtained by FLAC^{3D} for the reference case (i.e., $\varphi=17°$, $c=7$ kPa) that will be studied in the probabilistic analysis.

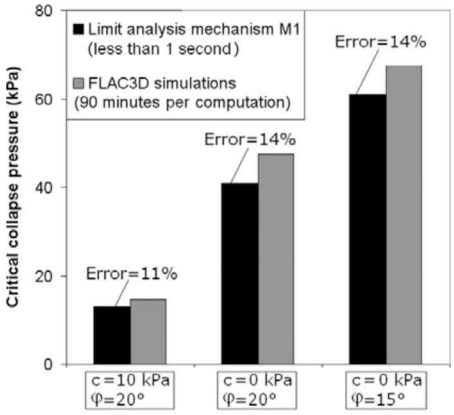

a. Critical collapse pressure

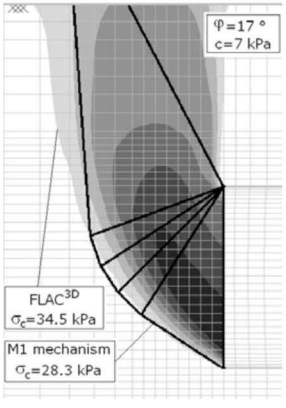

b. Failure pattern in the (y, z) plane

Fig. 6. Comparison between FLAC^{3D} numerical simulations and limit analysis

Probabilistic Numerical Results

The present collapse failure mechanism M1 will be used in all subsequent probabilistic analyses since (1) it gives better upper-bound solutions than the mechanism by Leca and Dormieux (1990) and (2) it gives results that are not very far from the solutions given by complex 3D numerical simulations using FLAC^{3D}.

The probabilistic numerical results presented in this paper consider the case of a circular tunnel with a diameter $D=10$ m and a cover $C=10$ m (i.e., $C/D=1$). The soil has a unit weight of 18 kN/m^3. No surcharge loading ($\sigma_s=0$) is considered in the analysis.

For the probability distribution of the random variables, two cases are studied. In the first case, referred to as *normal* variables, c and φ are considered as normal variables. In the second case, referred to as *nonnormal* variables, c is assumed to be lognormally distributed while φ is assumed to be bounded and a β distribution is used (Fenton and Griffiths 2003). The parameters of the β distribution are determined from the mean value and standard deviation of φ (Haldar and Mahadevan 2000). For both cases, correlated and uncorrelated variables are considered. In this paper, the illustrative values used for the statistical moments of the shear strength parameters and their coefficient of correlation $\rho_{c,\varphi}$ are as follows: $\mu_c=7$ kPa, $\mu_\varphi=17°$, $\mathrm{COV}_c=20\%$, $\mathrm{COV}_\varphi=10\%$, and $\rho_{c,\varphi}=-0.5$.

A common approach to determine the reliability index of a stability problem (slope stability, bearing capacity, etc.) is based on the calculation of the reliability index corresponding to the deterministic failure surface (i.e., the one corresponding to the minimum safety factor or the ultimate load) (Christian et al. 1994). In this paper, the reliability index is determined by minimizing the quadratic form of Eq. (9) not only with respect to the random variables, but also with respect to the geometrical parameters of the failure mechanism (α,β_i) $i=1,..,n-1$ (Bhattacharya et al. 2003; Youssef Abdel Massih 2007; Youssef Abdel Massih et al. 2008). Five rigid blocks (i.e., $n=5$ in Fig. 2) are considered.

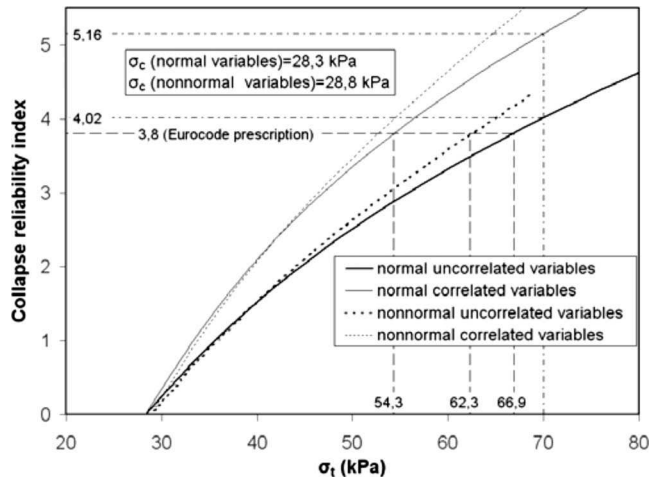

Fig. 7. Reliability index versus σ_t for normal, nonnormal, uncorrelated, and correlated variables

Therefore, the minimization is performed with respect to *seven* parameters $(\alpha, \beta_i, c, \varphi)$. The surface obtained corresponding to the minimum reliability index is referred to here as the critical probabilistic surface.

For the configuration presented earlier, the tunnel collapse pressure corresponding to normal variables was found equal to σ_c=28.3 kPa. However, for nonnormal variables, the collapse pressure was computed using the equivalent mean values of the random variables and was found equal to 28.8 kPa.

Reliability Index, Critical Dispersion Ellipses, and Partial Safety Factors

Fig. 7 presents the Hasofer-Lind reliability index versus the applied pressure σ_t for four combinations of *normal* and *nonnormal*, uncorrelated and correlated shear strength parameters. For all cases, the reliability index increases with the increase of the tunnel face pressure σ_t. The comparison of the results of correlated variables with those of uncorrelated variables shows that the reliability index corresponding to uncorrelated variables is smaller than the one of negatively correlated variables for both *normal* and *nonnormal* variables. One can conclude that assuming uncorrelated shear strength parameters is conservative in comparison to assuming negatively correlated parameters. For a target reliability index of 3.8 as imposed by Eurocode 7, the required tunnel pressure is smaller for correlated and nonnormal variables. For instance, with respect to the reference case of normal and uncorrelated variables, σ_t decreases by 19% if the variables are correlated (54.3 kPa to be compared to 66.9 kPa) and by 7% if the variables are considered to follow nonnormal distributions (62.3 kPa to be compared to 66.9 kPa).

The values (c^* and φ^*) of the design points corresponding to different values of the tunnel face pressure σ_t can give an idea about the partial safety factors of each of the strength parameters c and $\tan\varphi$ as follows:

$$F_c = \frac{\mu_c}{c^*} \tag{12}$$

$$F_\varphi = \frac{\tan(\mu_\varphi)}{\tan\varphi^*} \tag{13}$$

Table 2 gives the obtained partial safety factors F_c and F_φ and the corresponding design point and reliability index for the four combinations of normal, nonnormal, uncorrelated, and correlated variables and for different values of the tunnel face pressure σ_t. This table also shows the empirical F_c and F_φ values suggested by Eurocode 7. For a reliability index close to 3.8 as suggested by Eurocode 7 in the ULS, the values obtained from the present approach for the four combinations of assumptions are between 1 and 1.5 for F_c and about 1.5 for F_φ. The corresponding Eurocode values are 1.6 and 1.25. As can be seen, contrary to Eurocode 7, the present probabilistic approach attributes more safety to the cohesion parameter than Eurocode 7.

Table 2. Reliability Index, Design Point, and Partial Safety Factors

σ_t	β_{HL}	c^*	φ^*	F_c	F_φ
Normal uncorrelated variables					
28.3	0.00	7.00	17.00	1.00	1.00
30	0.25	6.76	16.69	1.04	1.02
35	0.93	6.18	15.78	1.13	1.08
40	1.53	5.74	14.90	1.22	1.15
50	2.51	5.19	13.33	1.35	1.29
60	3.32	4.82	12.02	1.45	1.44
70	4.02	4.53	10.87	1.55	1.59
80	4.63	4.30	9.85	1.63	1.76
100	5.69	3.95	8.07	1.77	2.16
Normal correlated variables					
28.3	0.00	7.00	17.00	1.00	1.00
30	0.35	6.79	16.66	1.03	1.02
35	1.30	6.38	15.57	1.10	1.10
40	2.11	6.32	14.40	1.11	1.19
50	3.35	6.54	12.37	1.07	1.39
60	4.34	6.82	10.73	1.03	1.61
70	5.16	7.11	9.34	0.98	1.86
80	5.87	7.40	8.12	0.95	2.14
100	7.08	7.94	6.05	0.88	2.88
Nonnormal uncorrelated variables					
28.8	0.00	7.00	17.00	1.00	1.00
30	0.17	6.71	16.75	1.04	1.02
35	0.89	6.19	15.77	1.13	1.08
40	1.53	5.84	14.81	1.20	1.16
50	2.63	5.42	13.17	1.29	1.31
60	3.58	5.12	11.82	1.37	1.46
Nonnormal correlated variables					
28.8	0.00	7.00	17.00	1.00	1.00
30	0.24	6.73	16.72	1.04	1.02
35	1.23	6.40	15.56	1.09	1.10
40	2.08	6.33	14.39	1.11	1.19
50	3.47	6.33	12.51	1.11	1.38
60	4.65	6.33	11.04	1.11	1.57

For σ_t=70 kPa (Fig. 7), the collapse reliability index for uncorrelated and correlated normal variables are respectively equal to 4.02 and 5.16. The corresponding most probable failure points obtained from the minimization procedure (Table 2) are found to be at (c^*=4.53 kPa, φ^*=10.87°) and (c^*=7.11 kPa, φ^*=9.34°). These are the points of tangency of the critical dispersion ellipses with the limit state surface. Notice that the limit state surface divides the combinations of (c, φ) that would lead to failure from the combinations that would not. The (c, φ) values defining the

Int. J. Geomech. 2009.9:237-249.

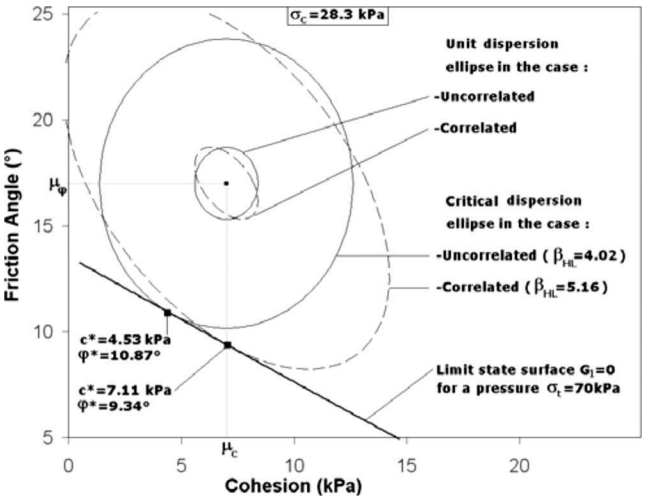

Fig. 8. Unit and critical dispersion ellipses for correlated and uncorrelated variables in the physical space of the random variables

limit state surface are obtained by searching c (or φ) for a prescribed φ (or c) that achieve both the conditions (1) $G_1=0$ where G_1 is defined by Eq. (7) and (2) the collapse pressure σ_c in Eq. (7) is obtained by a maximization with respect to the geometrical parameters of the failure mechanism. For this purpose, a numerical procedure was coded in Microsoft Excel Visual Basic. It calls the Excel Solver iteratively in order to simultaneously satisfy the two preceding conditions. Fig. 8 provides graphical representation of the reliability analysis for both correlated and uncorrelated shear strength parameters in the physical space of the random variables. One can easily see that negative correlation between shear strength parameters rotates the major axis of the ellipse from the vertical direction.

The critical probabilistic failure mechanisms obtained for both uncorrelated and negatively correlated variables are plotted in Fig. 9 using the values c^* and φ^* of the design point (Table 2) and the corresponding critical angular parameters of the failure mechanism. One can observe that the most probable failure mechanisms in the two cases are much more "extended" than the critical failure mechanism obtained in the deterministic analysis by optimization of the tunnel pressure with respect to the geometrical parameters of the failure mechanism. This is due to the fact that the probabilistic failure mechanisms correspond to a smaller value of φ. Thus, contrary to the critical failure mechanism obtained in the deterministic analysis, the probabilistic failure mechanism outcrops the ground surface for both uncorrelated and negatively correlated shear strength parameters.

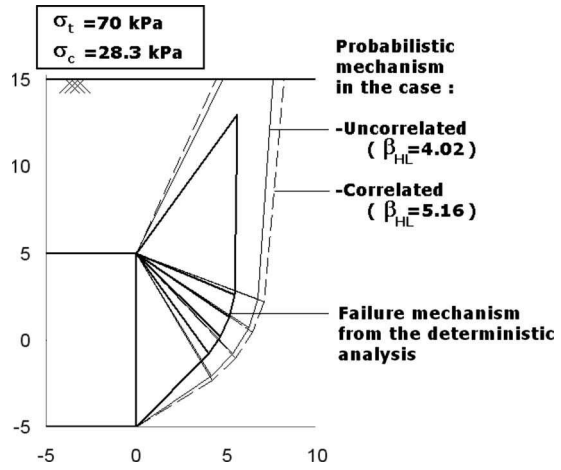

Fig. 9. Critical collapse mechanisms in the (y,z) plane

Failure Probability

Both MC and IS simulations were performed for the computation of the failure probability. In this paper, these simulations were carried out in the standardized space of uncorrelated variables. Hence, only uncorrelated normal random variables have been generated. The IS density function used in the standard uncorrelated space is given as follows (e.g., Lemaire 2005):

$$f(u)=\frac{1}{\sqrt{2\pi}}e^{-1/2(u-u^*)^2} \tag{14}$$

where u^*=transformed value of the design point in the standard uncorrelated space of the random variables. When studying nonnormal and/or correlated variables, the limit state surface, which is determined point by point as explained in the previous section, was transformed to the standardized space of uncorrelated normal variables using the equivalent normal transformation (i.e., the Rackwitz-Fiessler equations) for each couple of (c,φ). The two equations used for the transformation of each (c,φ) of the limit state surface from the physical space to the standardized normal uncorrelated space (u_1,u_2) are (Lemaire 2005)

$$u_1=\left(\frac{c-\mu_c^N}{\sigma_c^N}\right) \tag{15}$$

$$u_2=\frac{1}{\sqrt{1-\rho^2}}\left[\left(\frac{\varphi-\mu_\varphi^N}{\sigma_\varphi^N}\right)-\rho\left(\frac{c-\mu_c^N}{\sigma_c^N}\right)\right] \tag{16}$$

where ρ=coefficient of correlation of c and φ, and μ_c^N, μ_φ^N, σ_c^N, and σ_φ^N=respectively, the equivalent normal means and standard deviations of the random variables c and φ. They are determined from the translation approach using the following equations:

$$\frac{c-\mu_c^N}{\sigma_c^N}=\Phi^{-1}[F_c(c)] \tag{17}$$

$$\frac{\varphi-\mu_\varphi^N}{\sigma_\varphi^N}=\Phi^{-1}[F_\varphi(\varphi)] \tag{18}$$

where F_c and F_φ=non-Gaussian cumulative distribution functions (CDFs) of c and φ, and $\Phi^{-1}(\cdot)$=inverse of the standard normal cumulative distribution. If desired, the original correlation matrix (ρ_{ij}) of the nonnormals can be modified to ρ'_{ij} in line with the equivalent normal transformation, as suggested in Der Kiureghian and Liu (1986). Some tables of the ratio ρ'_{ij}/ρ_{ij} are given in Appendix B2 of Melchers (1999). For the cases illustrated herein, the correlation matrix, thus modified, differs only slightly from the original correlation matrix. Hence for simplicity, the examples of this study retain the original unmodified correlation matrices (Low et al. 2007).

Figs. 10 and 11 present, respectively, the failure probability and the corresponding coefficient of variation versus the number of samples as given by MC and IS for normal and nonnormal correlated variables. The tunnel face pressure was equal to 50 kPa. The expressions used for the computation of the failure probability and the corresponding coefficient of variation in both MC and IS simulations are given by Eqs. (3)–(6). A computer program

Int. J. Geomech. 2009.9:237-249.

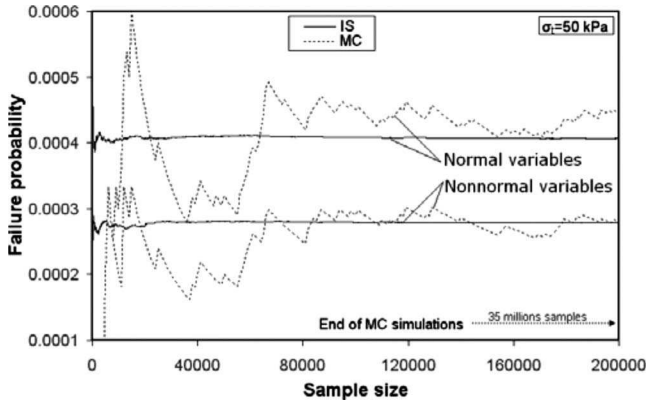

Fig. 10. Failure probability versus the number of samples for correlated variables as given by IS and MC

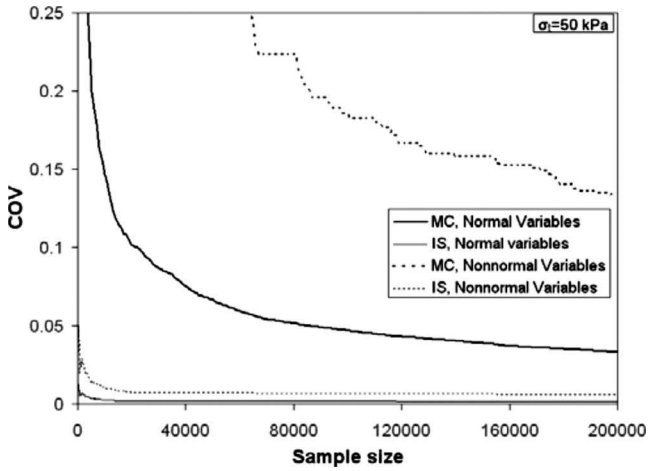

Fig. 11. Coefficient of variation of the failure probability versus the number of samples for correlated variables as given by IS and MC

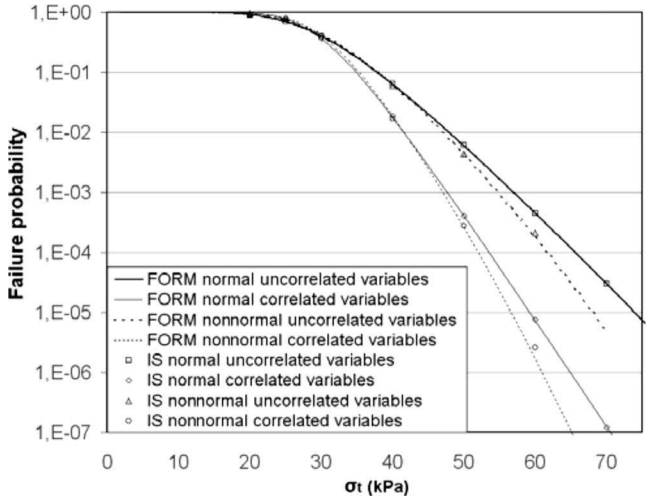

Fig. 12. Comparison of the failure probability as given by FORM and IS

has been written in Microsoft Excel Visual Basic for these computations. It should be mentioned that for the MC simulations, a single set of samples was generated for the estimation of the failure probability. This is because the difference between the two studied cases was taken into account through the transformation of the limit state surface from the physical space to the rotated standard normal uncorrelated (u_1, u_2) space using Eqs. (15)–(18). Also, the same set of samples can be used for uncorrelated variables and for different values of the tunnel applied pressure σ_t. Notice however that in the IS method, a new set of samples was generated for each probability distribution (normal and nonnormal) and correlation coefficient and for each value of the applied pressure. This is because the design point changes with the probability distribution and correlation of the random variables and with the value of the tunnel applied pressure σ_t. Finally, notice that the determination of the reliability index for use in the IS simulations was determined using the dispersion ellipsoid approach presented earlier.

Figs. 10 and 11 show that the convergence of the failure probability calculated by IS is obtained for a sample size of 20,000 with a coefficient of variation smaller than 1%. This value of the coefficient of variation is much smaller than the commonly adopted value used in the literature, i.e., 10%. In order to have a clear visualization of the convergence of the IS method, the maximal number of samples represented on the x-axis of Figs. 10 and 11 was limited to 200,000. For the MC simulation, a sample size of 5,000,000 was necessary to achieve an almost constant value of the failure probability. The corresponding coefficient of variation was smaller than 3%. Notice however that 35,000,000 samples were necessary to achieve a coefficient of variation smaller than 1%. Finally, notice that similar trends were obtained in the case of uncorrelated normal and nonnormal variables (the figures are not shown in the paper) and the same conclusions cited earlier remain valid in the case of uncorrelated variables (i.e., an almost constant value of P_f was obtained from MC simulations beyond 5,000,000 samples ; however, a smaller coefficient of variation of 1% was obtained in the present case). In the following, only IS simulation method will be used since it gives close results with the MC simulations with a smaller sample size. All the subsequent results will be given for a maximal value of 1% for the coefficient of variation of the estimator.

By varying the applied pressure on the tunnel face, the reliability index was calculated and the failure probability was plotted in Fig. 12 using FORM approximation and IS simulations for normal, nonnormal, uncorrelated, and correlated variables. From this figure, it is observed that the failure probability obtained from FORM approximation are in good agreement with those obtained from IS simulations for the commonly used values of the coefficients of variation of the soil shear strength parameters (i.e., COV_c=20%, COV_φ=10%). This means that FORM approximation is an acceptable approach for estimating the failure probability for the commonly used values of the soil variability. It will be used in all subsequent computations.

In order to explain the good agreement between the two approaches, the limit state surface is plotted. Fig. 13 shows the limit state surface corresponding to a tunnel face pressure σ_t=50 kPa for normal and nonnormal uncorrelated random variables in the standard space of normal uncorrelated variables. This figure also shows the linear FORM approximation, which is tangent to the limit state surface at the design point. From this figure, it can be shown that the linear FORM approximation is very close to the exact limit state surface within the circle centered at the origin of the rotated and transformed space and having a radius equal to 3.

Int. J. Geomech. 2009.9:237-249.

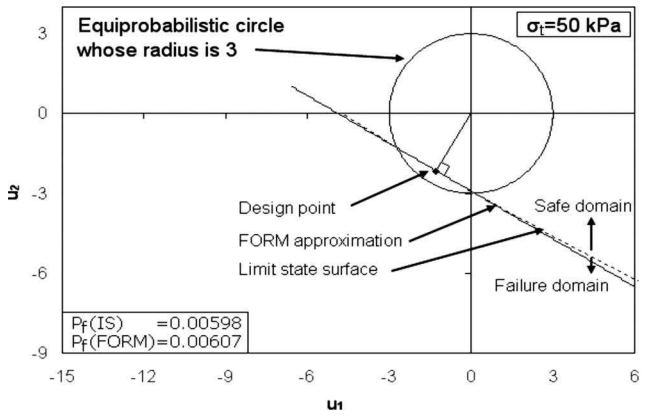

a. *Normal* variables

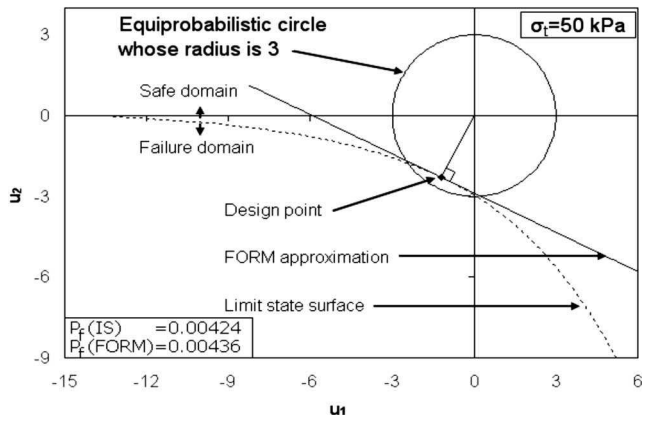

b. *Nonnormal* variables

Fig. 13. Limit state surface and FORM approximation in the uncorrelated case

This explains why a good agreement between the two approaches is obtained especially for normal variables. In the case of uncorrelated variables, the difference between the two failure probabilities given by FORM and IS is about 1.6% for normal variables and becomes equal to 3.0% for nonnormal variables (Fig. 13).

Sensitivity Analysis

Fig. 14 presents the CDFs of the tunnel face pressure for normal, nonnormal, correlated, and uncorrelated variables as given by FORM. When no correlation between shear strength parameters is considered, one can notice a more spread out CDF of the applied pressure (i.e., a higher coefficient of variation of this pressure) with respect to the case of correlated shear strength. The chosen probability distribution (i.e., normal, lognormal, and β distribution) does not significantly affect the values of the failure probability.

Fig. 15 presents the effect of the coefficient of variation of the shear strength parameters on the failure probability. It can be seen that a small change in the coefficient of variation of φ highly affects the failure probability. On the other hand, this failure probability is less sensitive to changes in the uncertainty of the cohesion. Thus, the failure probability is highly influenced by the coefficient of variation of φ. The greater the scatter in φ, the higher the failure probability. This means that accurate determination of the uncertainties of the angle of internal friction φ is very important in obtaining reliable probabilistic results.

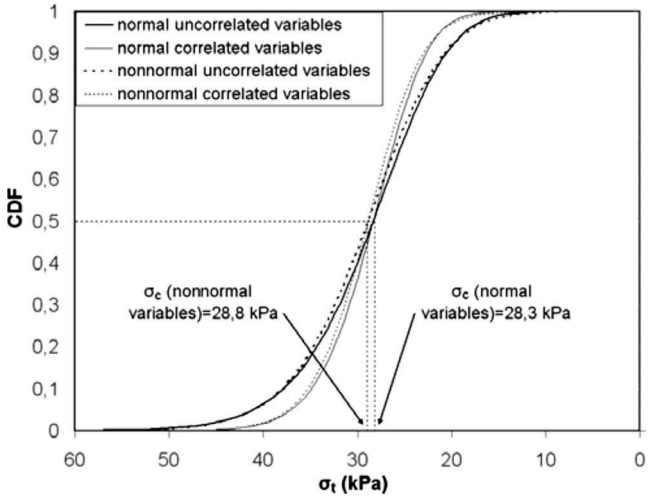

Fig. 14. CDFs of the tunnel face pressure

Probability Density Function of the Tunnel Face Pressure

Fig. 16 shows the PDFs corresponding to the CDFs given in Fig. 14. The PDFs were determined by numerical derivation of the CDFs. It can be seen that the results of normal and nonnormal variables are nearly similar. The correlation between the variables has on the contrary an important influence, making the probability density more significant around the deterministic value of the applied pressure. By fitting the PDF of the tunnel pressure to an empirical PDF (normal, lognormal, gamma) as shown in Fig. 17, it was found (after minimization of the sum of the relative errors between the values of the computed PDF and those of the empirical distribution) that the lognormal distribution is the one that best fits the computed PDF especially in the distribution tail of interest to the engineering practice (i.e., where $\sigma_t > 2\sigma_c$). It is then easy to use the lognormal CDF to determine the failure probability for a given applied tunnel pressure.

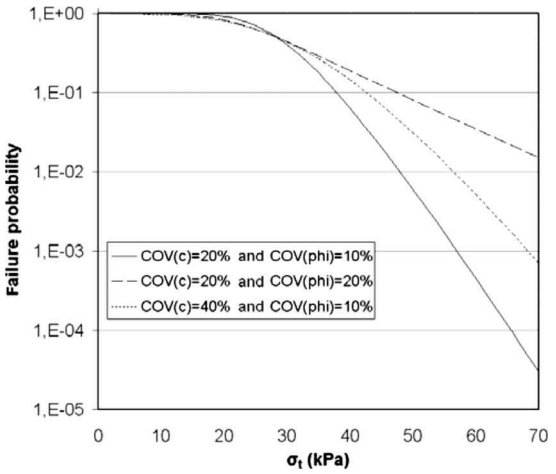

Fig. 15. Comparison of failure probabilities for different values of the coefficients of variation of c and φ

Int. J. Geomech. 2009.9:237-249.

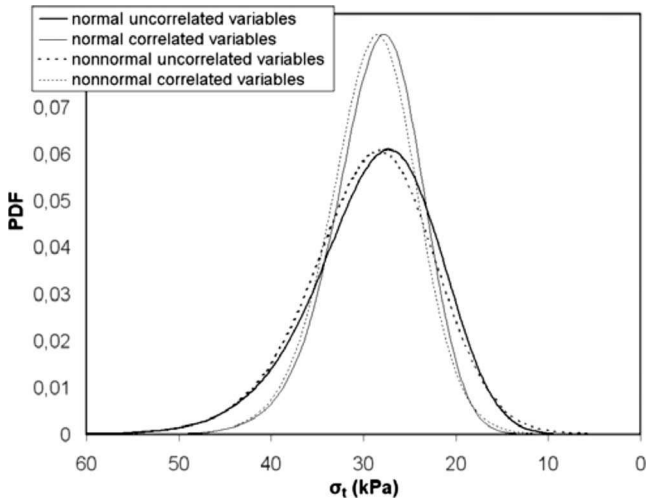

Fig. 16. PDFs of the tunnel face pressure

Reliability-Based Design

A reliability-based design (RBD) has been performed in this section. It consists of the calculation of the required tunnel face pressure for a target collapse reliability index of 3.8 as suggested by Eurocode 7 for the ULS. This tunnel pressure is called hereafter "probabilistic tunnel pressure."

Fig. 18 presents the probabilistic tunnel pressure for different values of the coefficients of variation of the shear strength parameters and their coefficient of correlation when the random variables follow normal distributions. This figure also presents the deterministic tunnel face pressure (56.6 kPa) corresponding to a safety factor against collapse ($F_s=\sigma_t/\sigma_c$) equal to 2. The probabilistic tunnel face pressure decreases with the decrease of the coefficients of variation of the shear strength parameters and the increase of the negative correlation between these parameters. It can become smaller than the deterministic tunnel face pressure for some values of the soil variability (i.e., $COV_\varphi=5\%$, $COV_c=20\%$). However, for high values of the coefficients of variation, the required tunnel face pressure is much higher than the deterministic value. As a conclusion, the deterministic tunnel face pressure may be higher or lower than the reliability-based tunnel face pressure, depending on the uncertainties of the random variables and the correlation between these variables.

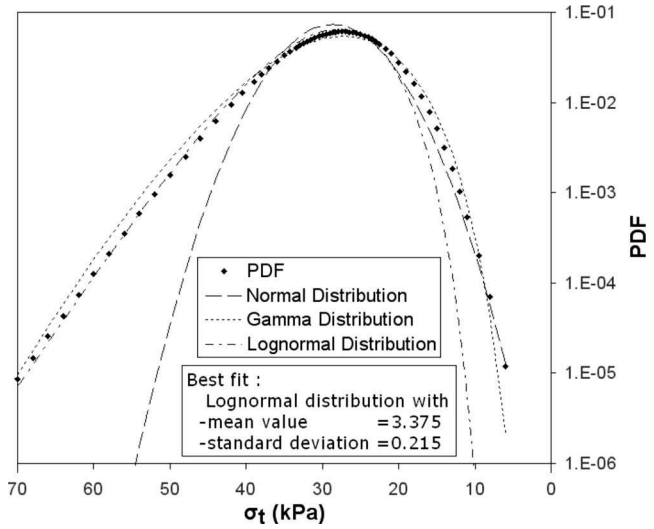

Fig. 17. Fit of the PDF of the tunnel pressure in the normal uncorrelated case

Conclusions

A reliability-based analysis and design of the face stability of a shallow circular tunnel driven by a pressurized shield was performed. Only the collapse and the blow-out failure modes of the ULS were studied. Two rigorous deterministic models based on the upper-bound method of limit analysis were used. It was shown that

- Although the results given by the upper-bound approach in limit analysis are unsafe estimates of the collapse and blow-out loads, they are the best ones compared to the available solutions in both the active and passive cases. This is because the present mechanisms provide greater solutions than those given by Leca and Dormieux (1990) in the collapse case and smaller results than those of these writers in the case of blow-out.
- The blow-out mode of failure does not occur for the cases currently encountered in practice. Hence, only the collapse failure mode was considered in the probabilistic analysis and design against face stability.
- The present limit analysis results obtained from the M1 collapse mechanism are not very far from the solutions given by complex 3D numerical simulations using $FLAC^{3D}$.
- The collapse reliability index increases with the increase of the tunnel face pressure.
- FORM approximation is an acceptable approach for estimating the failure probability against collapse for the commonly used values of the soil variability.
- The assumption of uncorrelated shear strength parameters was found conservative (i.e., it gives a greater failure probability) in comparison to that of negatively correlated parameters; however, the type of the probability distribution does not significantly affect the values of the failure probability.
- The failure probability is more sensitive to φ than to c. The greater the scatter in φ, the higher the failure probability. This means that the accurate determination of the uncertainties of the angle of internal friction φ is important in obtaining reliable probabilistic results.
- When no correlation between shear strength parameters is considered, a more spread out CDF of the tunnel pressure was obtained in comparison to the case of correlated shear strength parameters.
- The distribution of the PDF of the tunnel pressure was found very close to a lognormal distribution. This allows one to easily determine the failure probability against collapse for a given face pressure.
- A RBD has shown that the tunnel pressure determined probabilistically decreases with the increase of the negative correlation between the shear strength parameters and the decrease of their coefficients of variation.

Appendix. Computation of the Tunnel Collapse Pressure—M1 Mechanism

The formulation is given here for a five-block mechanism. The formulation for another number of blocks is straightforward.

Int. J. Geomech. 2009.9:237-249.

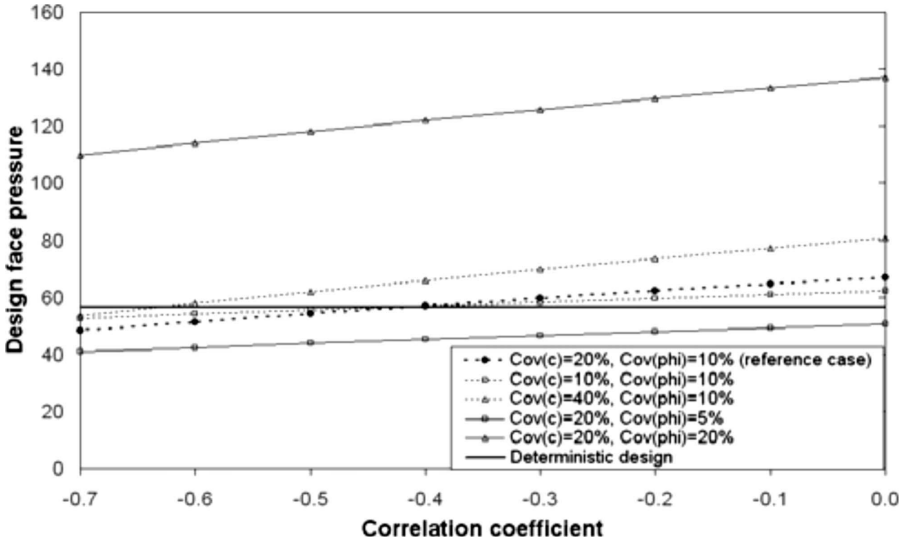

Fig. 18. Comparison between deterministic and probabilistic design pressures

Geometry

The distance from the extremity of each block i to the tunnel crown (h_i) and the height of the extremity of the last block (h'_5) are given by [Fig. 2(a)]

$$h'_5 = h_5 \cdot \frac{\sin(2\beta_4 + 2\beta_2 + \alpha - \varphi)}{\cos(\Psi_{4,5} - \varphi)} - \left(H - \frac{D}{2}\right) \tag{19}$$

$$\text{with} \begin{cases} h_2 = D \cdot \dfrac{\cos(\alpha + \varphi) \cdot \cos(\beta_1 - \alpha + \varphi)}{\sin(2\varphi)} \\ h_i = h_2 \cdot \displaystyle\prod_{k=2}^{i-1} \left[\frac{\cos(\Psi_{k,k+1} + \varphi)}{\cos(\Psi_{k-1,k} - \varphi)} \right] \quad \text{for} \quad i \geqslant 3 \end{cases} \tag{20}$$

The volumes of the extreme blocks (first and fifth blocks) are

$$V_1 = \frac{A_1 \cdot h_1 - A_{1,2} \cdot h_2}{3} \tag{21}$$

$$V_5 = \frac{A_{4,5} \cdot h_5 - A_5 \cdot h'_5}{3} \tag{22}$$

The volume of an intermediate block i (for $2 \leqslant i \leqslant 4$) is

$$V_i = \frac{A_{i-1,i} \cdot h_i - A_{i,i+1} \cdot h_{i+1}}{3} \tag{23}$$

If $h'_5 > 0$, the value of the outcropping surface of the fifth block is

$$A_5 = \frac{\Pi}{\cos(\varphi)} \cdot \left(\frac{h'_5 \cdot \sin(2\varphi)}{2 \sin(2\beta_4 + 2\beta_2 + \alpha + \varphi) \cdot \sin(2\beta_4 + 2\beta_2 + \alpha - \varphi)} \right)^2 \cdot \sqrt{\frac{\sin(2\beta_4 + 2\beta_2 + \alpha + \varphi)}{\sin(2\beta_4 + 2\beta_2 + \alpha - \varphi)}} \tag{24}$$

Otherwise, the mechanism does not outcrop and $A_5 = 0$.

The area of the elliptical surface resulting from the intersection of the first cone (adjacent to the tunnel face) with the circular tunnel face is

$$A_1 = \frac{\Pi \cdot D^2}{4 \cos(\varphi)} \cdot \sqrt{\cos(\alpha - \varphi) \cdot \cos(\alpha + \varphi)} \tag{25}$$

The area of the contact elliptical surface between two successive blocks i and $i+1$ is given by

$$\begin{cases} A_{1,2} = \dfrac{\Pi \cdot D^2}{4 \cos(\varphi)} \cdot \cos(\alpha + \varphi)^2 \cdot \dfrac{\sqrt{\cos(\beta_1 - \alpha + \varphi)}}{\cos(\beta_1 - \alpha - \varphi)^{1.5}} \\ A_{i,i+1} = \dfrac{\Pi \cdot D^2}{4 \cos(\varphi)} \cdot \cos(\alpha + \varphi)^2 \cdot \dfrac{\sqrt{\cos(\Psi_{i,i+1} + \varphi)}}{\cos(\Psi_{i,i+1} - \varphi)^{1.5}} \cdot \displaystyle\prod_{k=2}^{i} \left[\frac{\cos(\Psi_{k-1,k} + \varphi)^2}{\cos(\Psi_{k-1,k} - \varphi)} \right] \quad \text{for} \quad i \geqslant 2 \end{cases} \tag{26}$$

Kinematics

The velocity of the block i and the relative velocity between the blocks i and $i+1$ are

$$v_i = v_1 \cdot \prod_{k=2}^{i} \frac{\cos(\Psi_{k-1,k} + \varphi)}{\cos(\Psi_{k-1,k} - \varphi)} \quad \text{for} \quad i \geqslant 2 \tag{27}$$

$$v_{i,i+1} = v_i \cdot \frac{\sin(2\Psi_{i,i+1})}{\cos(\Psi_{i,i+1} - \varphi)} \quad \text{for} \quad i \geqslant 1 \tag{28}$$

$$\text{where} \begin{cases} \Psi_{0,1} = \alpha \\ \Psi_{i,i+1} = \beta_i - \Psi_{i-1,i} \quad \text{for} \quad i \geqslant 1 \end{cases} \tag{29}$$

Int. J. Geomech. 2009.9:237-249.

Expressions of Nγ and Ns

For a five-block collapse mechanism, the critical collapse pressure can be calculated from Eqs. (10) and (11), with

$$N_\gamma = \frac{P_{31} + P_{41} + P_{51} + P_{52}}{D} \tag{30}$$

$$N_s = \frac{\frac{v_5}{v_1} \cdot \sin(2\beta_2 + 2\beta_4 + \alpha) \cdot A_5}{A_1 \cdot \cos(\alpha)} \tag{31}$$

$$\text{where} \quad P_{51} = \frac{\frac{v_4}{v_1} \cdot \sin(2\beta_1 + 2\beta_3 - \alpha) \cdot V_4}{A_1 \cdot \cos(\alpha)} \tag{32}$$

$$P_{52} = \frac{\frac{v_5}{v_1} \cdot \sin(2\beta_2 + 2\beta_4 + \alpha) \cdot V_5}{A_1 \cdot \cos(\alpha)} \tag{33}$$

$$P_{41} = \frac{\frac{v_2}{v_1} \cdot \sin(2\beta_1 - \alpha) \cdot V_2 + \frac{v_3}{v_1} \cdot \sin(2\beta_2 + \alpha) \cdot V_3}{A_1 \cdot \cos(\alpha)} \tag{34}$$

$$P_{31} = \frac{V_1 \cdot \sin(\alpha)}{A_1 \cdot \cos(\alpha)} \tag{35}$$

References

Baecher, G. B., and Christian, J. T. (2003). *Reliability and statistics in geotechnical engineering*, Wiley, New York.

Bhattacharya, G., Jana, D., Ojha, S., and Chakraborty, S. (2003). "Direct search for minimum reliability index of earth slopes." *Comput. Geotech.*, 30, 455–462.

Chen, W. F. (2008). *Limit analysis and soil plasticity*, J. Ross Publishing Classics, 637.

Christian, J., Ladd, C., and Baecher, G. (1994). "Reliability applied to slope stability analysis." *J. Geotech. Eng.*, 120(12), 2180–2207.

Der Kiureghian, A., and Liu, P. L. (1986). "Structural reliability under incomplete probability information." *J. Eng. Mech.*, 112(1), 85–104.

Ditlevsen, O. (1981). *Uncertainty modelling: With applications to multidimensional civil engineering systems*, McGraw-Hill, New York.

Fenton, G. A., and Griffiths, D. V. (2003). "Bearing capacity prediction of spatially random C-φ soils." *Can. Geotech. J.*, 40, 54–65.

Haldar, A., and Mahadevan, S. (2000). *Probability, reliability and statistical methods in engineering design*, Wiley, New York.

Hasofer, A. M., and Lind, N. C. (1974). "Exact and invariant second-moment code format." *J. Engrg. Mech. Div.*, 100(1), 111–121.

Leca, E., and Dormieux, L. (1990). "Upper and lower bound solutions for the face stability of shallow circular tunnels in frictional material." *Geotechnique*, 40(4), 581–606.

Lemaire, M. (2005). *Fiabilité des structures, Hermès*, Lavoisier, Paris (in French).

Low, B. K., Lacasse, S., and Nadim, F. (2007). "Slope reliability analysis accounting for spatial variation." *Georisk: Assessment and management of risk for engineered systems and geohazards*, 1(4), Taylor & Francis, London, 177–189.

Low, B. K., and Tang, W. H. (1997a). "Efficient reliability evaluation using spreadsheet." *J. Eng. Mech.*, 123(7), 749–752.

Low, B. K., and Tang, W. H. (1997b). "Reliability analysis of reinforced embankments on soft ground." *Can. Geotech. J.*, 34, 672–685.

Low, B. K., and Tang, W. H. (2004). "Reliability analysis using object-oriented constrained optimization." *Struct. Safety*, 26, 69–89.

Melchers, R. E. (1999). *Structural reliability analysis and prediction*, 2nd Ed., Wiley, New York.

Mollon, G., Dias, D., and Soubra, A-H. (2009). "Probabilistic analysis of circular tunnels using a response surface methodology." *J. Geotech. Geoenviron. Eng.*, 135(9), 1314–1325.

Oberlé, S. (1996). "Application de la méthode cinématique à l'étude de la stabilité d'un front de taille de tunnel, *Final Project Rep. Prepared for ENSAIS*, Strasbourg, France (in French).

Phoon, K.-K., and Kulhawy, F. H. (1999). "Evaluation of geotechnical property variability." *Can. Geotech. J.*, 36, 625–639.

Rackwitz, R., and Fiessler, B. (1978). "Structural reliability under combined random load sequences." *Comput. Struct.*, 9(5), 484–494.

Soubra, A.-H. (1999). "Upper-bound solutions for bearing capacity of foundations." *J. Geotech. Geoenviron. Eng.*, 125(1), 59–68.

Youssef Abdel Massih, D. S. (2007). "Analyse du comportement des fondations superficielles filantes par des approches fiabilistes." Ph.D. thesis, Université of Nantes, Nantes, France (in French).

Youssef Abdel Massih, D. S., and Soubra, A.-H. (2008). "Reliability-based analysis of strip footings using response surface methodology." *Int. J. Geomech.*, 8(2), 134–143.

Youssef Abdel Massih, D. S., Soubra, A.-H., and Low, B. K. (2008). "Reliability-based analysis and design of strip footings against bearing capacity failure." *J. Geotech. Geoenviron. Eng.*, 134(7), 917–928.

Int. J. Geomech. 2009.9:237-249.